Mon. Not. R. Astron. Soc. **265,** 664–680 (1993)

On the nature of rapid X-ray variability in active galactic nuclei

A. R. Green, I. M. McHardy and H. J. Lehto★

Astronomy and Space Physics Group, Department of Physics, University of Southampton, Southampton SO9 5NH

Accepted 1993 June 7. Received 1993 June 5; in original form 1992 December 21

ABSTRACT

We systematically analyse all (110) *EXOSAT* AGN medium-energy light curves of length greater than 20 ks to search for and quantify their flux variability. We also perform extensive simulations to quantify the selection effects (such as the source brightness or the length of observation) that might prevent the detection of variability. We quantify variability in terms of a 'normalized variability amplitude' (*NVA*) derived from the power spectrum of each light curve. Of the 32 sources observed, we detect variability in 12. We find that, contrary to some previous claims, there is no evidence that sources change the character of their variability between observations.

We confirm that there is a strong inverse correlation between *NVA* and source luminosity which can be simply explained if source size scales with luminosity. A further result is that the sources with the steepest *energy* spectra are possibly the most variable. One explanation of the latter result, in the context of reprocessing models, might be that sources with steeper *energy* spectra contain a smaller reflected or reprocessed component, which might be expected to vary less rapidly than the direct component.

We briefly discuss a small number of light curves obtained using the low-energy telescope on *EXOSAT*, and confirm that their power spectra are steeper than those of the corresponding medium-energy light curves.

The power spectra are consistent with both multiple decay shot-noise models and with the rotating-spot models. In the case of the rotating-spot model we can place upper limits on the central black hole masses of typically a few $\times 10^7$ $M_\odot$. Starburst models cannot explain the observed rapid X-ray variability.

Key words: galaxies: active – galaxies: nuclei – X-rays: galaxies.

1 INTRODUCTION

The most generally accepted model for active galaxies (AGN) proposes that the power source, or 'central engine', consists of a massive black hole which generates energy either through accretion or, if the black hole is spinning, through the release of stored energy of rotation (e.g. Rees 1984). Unfortunately, despite some decades of observation, we are still far from determining most of the basic parameters of the central engine, such as the mass of the proposed black hole, the geometry of the emitting region(s) and the mechanisms by which radiation is produced. Studies of X-ray spectra and variability offer particular hope of understanding the central engine of AGN as, in most simple physical scenarios, X-rays should be generated within a few Schwarzschild radii of the black hole. The X-ray spectra of AGN have been discussed widely elsewhere (e.g. Turner & Pounds 1989). In this paper we concentrate on observations of X-ray variability.

By the early 1980s, it was known that long-time-scale (months–years) X-ray variability was fairly common, but the situation regarding shorter time-scale variability was not at all clear. For example, when AGN were observed with the *HEAO-A2* experiment, Tennant & Mushotzky (1983) concluded that 'large amplitude short timescale variations are not a characteristic of the X-ray emission from active galaxies'. Observations with *EXOSAT* began to change this view (e.g. McHardy 1985 and references therein), and by the late 1980s it was known that short-time-scale variability was actually very common (e.g. McHardy 1988, 1989). The major factor that lead to this breakthrough in understanding

★ Present address: Turku University Observatory, Tuorla, SF 21500 Piikkiö, Finland.

was the 4-d orbit of *EXOSAT* which allowed much longer uninterrupted observations than had been possible previously. The *EXOSAT* data base (see Giommi 1986 and Albrecht & Egret 1986 for details) is therefore a very valuable source of information about variability and provides the data for this paper.

Grandi et al. (1992) have already used the *EXOSAT* data base to search for variability in the Piccinotti et al. (1982) sample of hard X-ray selected AGN. Many of the sources discussed here are also discussed by Grandi et al., to whom the reader is referred for a comprehensive presentation of individual light curves. Grandi et al. concentrated on the detection or otherwise of variability, testing each light curve against a constant hypothesis using a χ^2 statistic, and detected variability in 12 out of 29 sources. Here we extend this work, particularly by examining the power spectra of *EXOSAT* AGN light curves.

Power spectrum analysis has long been used as a standard tool in the study of variability, but was first applied to the study of the X-ray variability of AGN by McHardy & Czerny (1987) and Lawrence et al. (1987). These first observations (of NGC 5506 and 4051 respectively) showed that there were no obvious periodicities and that the variability was, at least to first order, self-similar with power spectrum slopes of around 1–1.5. Subsequent work (e.g. McHardy 1988 and Lehto, McHardy & Abraham 1991) found broadly similar results for other AGN. The overall shapes of these power spectra provide strong constraints on any models for the emission of X-rays from AGN.

EXOSAT AGN light curves generally look very random, but their power spectra are not well fitted by simple shot-noise models. Other models that have been considered include a multiple shot-noise model (Lehto 1989a) and a model in which hotspots on the surface of an accretion disc are enhanced by relativistic effects (Abramowicz et al. 1991). The predictions of these models about the shape of the power spectra will be described, and tested, in later sections.

In the present paper we carefully and systematically analyse the light curves of 110 observations of 32 separate Seyfert galaxies and QSOs from the *EXOSAT* data base in order that both the frequency of occurrence of variability and the nature of the variability can be investigated. We perform a simple test for variability using a χ^2 statistic in a manner similar to that of Grandi et al., but also calculate the power spectra of all of the light curves. From these power spectra we study the amplitude of variability as a function of source luminosity using a 'normalized variability amplitude' (*NVA*; see Section 2). The *NVA* is a statistical measure of variability and so is better than any measurement based on a one-off flare or dip which might not be generally characteristic of the source.

For some sources (e.g. NGC 4593: Barr et al. 1987) it has been reported that the power spectra may vary from observation to observation. Such apparent variations could be a spurious effect of the short observation times involved. We therefore examine the question of whether X-ray variability is statistically stationary over long time-scales (Section 3.1). We also examine whether variability might be associated in any way with the *energy* spectrum of a source, and come up with a rather interesting result (Section 3.4.2).

Almost all of the light curves that we examine come from the medium-energy (ME) detectors on *EXOSAT* in the energy range 1–8 keV as this is the range over which the AGN *EXOSAT* light curves are generally of the highest signal-to-noise ratio. However, a small number of light curves from the low-energy (LE) imaging telescope are also discussed, and we examine possible lags between the medium- and low-energy light curves (Section 3.5). Finally, we discuss our results in the context of the two models mentioned above.

We note that an important part of our work is the extensive simulations that we have carried out to quantify the sensitivity of the sample to the detection of variability and to estimate the errors on the power spectrum slopes and on the *NVA* s.

2 SAMPLE SELECTION AND ANALYSIS

The aim of this study is to carry out a systematic search for variability in X-ray light curves of AGN and, once found, to quantify the precise nature of the variability. This study is limited to Seyfert galaxies and QSOs. We do not consider BL Lac objects, in which relativistic beaming almost certainly has a large effect on observed variability time-scales, but refer the reader to the work of Giommi et al. (1990).

The data considered here are, simply, all *EXOSAT* medium-energy AGN light curves of 'good quality' (see Section 2.3 for a definition of 'good quality'). We therefore consider more sources than are included in, for example, the Piccinotti sample studied by Grandi et al. (1992). As the majority of AGN included in the *EXOSAT* data base were observed initially for spectral, rather than timing, purposes and as the light curves of sources in the Piccinotti sample are anyway of variable quality, this extension of the sample introduces no biases but does increase the statistical significance of our conclusions.

It is important for a study of this type to use the most appropriate method of analysis. Many methods have been used for analysing AGN variability, including fractal functions (McHardy & Czerny 1987) and structure functions (Bregman et al. 1988). These methods have their merits in particular cases, but here it is found that power spectrum analysis is the most suitable method for quantifying the wide range of variability in the present sources. No analysis method, of course, is perfect, and two light curves that look different can have similar power spectrum shapes. However, the power spectrum method produces reasonably comprehensible results and has the added advantage that, as it has been widely used in the past, it is generally well understood, and so we are content to use it here.

Much of the previous work carried out in this field has been based on measurements of a 'doubling time-scale'. If the variations seen in the light curves of AGN are self-similar, as shown in McHardy & Czerny (1987) and Lawrence et al. (1987), then the doubling time-scale is meaningless. Even if the variations are not self-similar, many doubling time-scales have been determined from just one event, which will in all probability be atypical of the general behaviour of the source. We suggest that a good measure of the variability is the normalized variability amplitude (*NVA*), as defined in McHardy (1988). The *NVA* is the square root of the power at a specific frequency, normalized to the mean count rate of that light curve (which is effectively the same as normalizing the light curve to the mean and then calculating the power

spectrum). The frequency chosen at which to sample the *NVA* is strongly governed by the individual power spectra. For the purposes of this paper we choose a frequency of 2×10^{-4} Hz (5000 s), which is high enough that it is a well-sampled frequency, but low enough that it is not dominated by the white-noise component, arising purely from limited photon-counting statistics, which is seen on all power spectra.

Now that our selection criteria have been broadly outlined we must define what we mean by 'good quality' data. This is achieved by simulating many light curves with a range of properties and determining from these simulations the properties a light curve must have in order for the probability of detecting variability to be high. These simulations are described below.

2.1 Method of analysis

The first piece of information that we need to obtain is whether a light curve is variable. For this purpose we use the χ^2 statistic to test the hypothesis that the flux is constant. We label the light curve as 'variable' if the hypothesis of constant flux is rejected at the >95 per cent confidence level. Otherwise sources are classed as 'constant'.

The power spectra of all the light curves are calculated whether the light curves are classed as variable by the χ^2 test or not. In all cases where the source flux is classed as being constant we find that the power spectrum is best fitted by a slope of approximately zero, i.e. the fluctuations in the light curve are purely statistical white noise caused by the uncertainty in measuring the flux.

The reasons for using the power spectrum as the main tool of analysis in this work have been discussed in the previous section. In this section, however, we will examine in more detail the main disadvantages of the power spectrum method, and describe the standard analysis used throughout this paper.

Most misinterpretation of power spectra is due to the fact that the measured power spectrum is actually the convolution of the window function and the true power spectrum (see Taghaferri et al. 1991 and Vio et al. 1992). The window function is defined as the power spectrum of unit-valued pulses with the same temporal distribution as the original time series (Deeming 1975). For equally sampled data the window function has a logarithmic slope of -2. Since the observed power spectrum is the convolution of the true power spectrum and the window function, if the true power spectrum has a slope steeper than -2 then the observed power spectrum will have a slope of -2 at high frequencies – i.e. it will be dominated by the window function if the effects of the window function are not removed. A further effect of the window function is the so-called 'red-noise leak'. As the time series is finite in length, the true power spectrum of the time series is convolved with the power spectrum of a boxcar function. This convolution has the effect of transferring power from the low frequencies to high frequencies (see Papadakis & Lawrence 1993, hereafter PL93, for a more detailed discussion of red-noise leak). If the time series is long, the effects of the red-noise leak are reasonably small and can be ignored. In this study, however, we use information from short observations and hence we must consider the effects the window function has on the observed power spectrum.

It is possible to remove the effects of the window function from the power spectrum using the CLEAN algorithm. The CLEAN algorithm we have used is described in Lehto (1989b, and 1993, in preparation) and is a development of that used by Roberts, Lehar & Dreher (1987).

The one-dimensional CLEAN algorithm used in time-series analysis is essentially the same as that commonly used in two-dimensional radio mapping, with the 1D window function being analogous to the 2D dirty beam and the 1D raw power spectrum being analogous to the 2D dirty map. The 1D CLEAN beam used is generally chosen to be a Gaussian with a half-power beamwidth (HPBW) equal to the HPBW of the window function. A full description of how the CLEAN algorithm works in synthesis mapping can be found in Högbom (1974) and Perley et al. (1985).

Although use of the CLEAN algorithm provides a good way of removing the effects of the temporal sampling from power spectra, the statistical properties of the CLEANed power spectra are not well determined, and hence it is necessary to use simulations to determine the expected errors on the power spectrum parameters. These simulations will be discussed in Section 2.5.

To obtain the power spectrum parameters (i.e. the power spectrum slope and *NVA*) from the CLEANed power spectrum we assume a model of the form

$$P = kf^{\alpha} + C \tag{1}$$

and fit this to the binned power spectrum (the validity of this model will be discussed in Section 2.5). The model of equation (1) assumes a simple power-law-type source flux variability ($=kf^{\alpha}$) together with a white-noise component due to the photon-counting statistics in the light curve (C). The *NVA* is calculated using the equation

$$NVA = \frac{\sqrt{k(2\times10^{-4})^{\alpha}}}{S}, \tag{2}$$

where k and α are as defined in equation (1) and S is the mean count rate for the light curve.

In order that we may fit the model described by equation (1) to the data, we logarithmically rebin the power spectrum into 10 bins per decade, and for the purposes of minimizing the fit statistic we use the spread of the original unbinned data points in each bin as the weight on the binned data point. Although these weights are a reasonable approximation to the errors in the binned data point it should be pointed out that the spread of the data in each bin is not exactly the true error on the data points, as the unbinned power spectrum estimates are not completely independent.

If the power spectrum is of the form $P\propto f^{\alpha}$ then PL93 showed that, in order to obtain unbiased estimates for the average power in each bin, it is necessary to bin the logarithm of the power spectrum. However, real power spectra do not follow the form $P\propto f^{\alpha}$ exactly; instead, the power is randomly distributed around the exact function $P=kf^{\alpha}+C$. This distribution of the power around $P=kf^{\alpha}+C$ follows the χ^2 distribution with 2 degrees of freedom which introduces a bias on the logarithmic power values, effectively reducing the numerical value of the binned power. It has

been shown by PL93 that the bias is constant for the χ^2 distribution, which means that the bias can be corrected for when taking the logarithm of the power spectrum.

The minimum frequency used in the fitting is given by $f_{\min}(\mathrm{Hz}) = 2.0/L_o$, where L_o is the observation length in seconds, which means that at least two full periods are present in the data.

Once the power spectrum has been logarithmically rebinned we fit the simple model of equation (1) to the power spectrum. We use a fit statistic that is similar to the χ^2 statistic in that the minimized statistic is the magnitude of the deviation of the fit from the data divided by the weight for each data point. The magnitude of the deviation of the fit from the data was calculated in logarithmic space, as otherwise the low-frequency points are weighted very heavily, even though they are intrinsically less accurate as the power spectrum is poorly sampled at low frequencies.

Once the power spectrum slope and normalization (with their relative errors) are known, the *NVA* can be calculated using equation (2). The errors in the *NVA* are determined from the errors in the power spectrum slope and normalization.

To summarize, we adopt a *standard analysis* which is performed on all the light curves (and used in all the simulations) and which takes the following form:

(i) the χ^2 probability that the light curve is a constant is calculated;
(ii) the CLEANed power spectrum is calculated;
(iii) the power spectrum is logarithmically rebinned and we fit the model shown in equation (1), and
(iv) the *NVA* is calculated from the model fit parameters.

2.2 The simulations

Many simulations have been carried out to determine the effects that the length and signal-to-noise ratio have on the detection of variability, to determine the probability of detecting variability in a particular light curve, and to deduce the errors on the power spectrum parameters for the variable sources in the sample.

All the simulations described in the following three sections were performed in the same way. First, a long light curve was constructed using the half-integral method outlined in Press (1978). In the limit where an 'infinite' number ($\geq$ few thousand) of data points are generated, the resulting power spectrum slope is theoretically pre-determined. Here we generate a light curve using 8192 data points. The resulting power spectrum slope was measured using a least-squares fit in logarithmic space and confirmed to be the same as the theoretical value.

Once the long light curve had been constructed, a section was randomly selected which was given the same temporal structure as the original observation (i.e. the observation to be simulated). The mean and standard deviation of the selected region of the long light curve were then normalized to the desired value (this value is different depending on the simulation and will be described for each of the simulations accordingly). A Poissonian noise component was then added to the light curve to simulate the effects of photon-counting statistics. The standard deviation of this Poissonian component was determined from the error bars on the original light curve. The simulated light curve was then analysed using the *standard analysis* outlined in the previous section.

2.3 Simulations to determine the effects of low flux and finite observation length on the detection of variability

It is important to know how the observation length and count rate influence the probability of the detection of variability. If the count rate is too low then the signal gets lost in the photon-counting noise which exists for all real light curves. If the observation is too short then there exists the possibility of confusion between weakly varying light curves and white-noise light curves (i.e. light curves that have a power spectrum of slope zero, but of power greater than that produced just by photon-counting statistics). If there are too few points in the light curve the power spectrum will be inherently noisy and it is impossible to determine the power spectrum accurately. In order to quantify these effects many simulations were carried out.

A variety of light curves with power spectrum slopes of -1.2 and similar properties to those found in the *EXOSAT* data base (i.e. of typical length 10–100 ks with 100-s time bins) were simulated as described above in Section 2.2. The simulated light curves were given typical *EXOSAT* time windows (i.e. short gaps about every 10 000 s where the detector swaps were made) and the standard deviation of the variability process was normalized to be either 0.1, 0.2 or 0.3 times the mean count rate. The mean count rate typically ranged between 0.45 and 12 count s^{-1}. Once the noise-free light curve had been constructed, a Poissonian noise component with a standard deviation between 0.5 and 0.9 count s^{-1} was added to the light curve to simulate the photon-counting statistics.

We actually used nine different values of the mean count rate and seven observation lengths. For each combination of mean count rate and observation length we constructed light curves with three different amplitudes of noise-free flux variations and three different amplitudes of photon-counting noise, making a total of 567 combinations of properties.

We simulated and analysed 25 different light curves for each of the 567 combinations of properties, giving a total of over 14 000 simulated light curves. From the results of the *standard analysis* outlined in Section 2.1 we could deduce the probability of detection for each combination of the light curve parameters.

It was found that the main limiting factors were the length of the observation and the ratio of mean count rate to the standard deviation of the photon-counting noise. The results of these extensive simulations show that in order that we might detect flux variations in a light curve at least 50 per cent of the time the light curve must satisfy the following conditions:

(i) the light curve must be longer than 20 ks, and
(ii) the mean count rate must be at least twice the standard deviation of the Poissonian noise (simulated photon-counting statistics).

To avoid the possible detection of spurious variability caused by bad data, we added a third constraint that the quality flag assigned to the light curve by the *EXOSAT* data base must be greater than 2 (3 is good and 5 is excellent). These three conditions define what we mean by 'good quality' data.

We searched the whole of the *EXOSAT* data base for light curves of AGN that satisfied these three conditions, finding 110 light curves of 32 sources. These are listed in Table 1.

2.4 The sensitivity of the sample to the detection of variability

There are a number of previous works relating to the detection of flux variability in AGN (e.g. Urry et al. 1987; Warwick 1986) but it has been difficult to assess the usefulness of these works as the authors have made no attempt to quantify the probability of detecting variability in any of the light curves used. For instance, Urry et al. considered observations of 64 galaxies made with the *Einstein Observatory* and concluded that rapid flux variability was detected in only three sources. This seems to be a low percentage, but, when we consider that the average source fluxes were in the range 0.0028 to 2.8 count s^{-1} and that the observation lengths ranged between 0.417 and 10.6 ks, we see that the sensitivity to detection varies hugely over the sample. In the absence of any measure of the sensitivity of the sample to detection it is therefore very difficult to draw any strong conclusions from this work.

In our sample we also suffer from problems of wide-ranging sensitivity to the detection of variability. In an attempt to quantify our sensitivity to the detection of variability we introduce a parameter called the 'detectable variability' (DV). This parameter is specific to an individual light curve and depends on the mean count rate, the observation length, and the amplitude of the photon-counting noise. The DV is deduced from simulations of light curves with different amplitudes of noise-free flux variations but with the same temporal structure, mean count rate, and photon-counting noise level as the observed light curve.

We define the DV as the variability a light curve must have to satisfy the conditions for the detection of variability outlined above (the hypothesis of the light curve being constant is rejected at the >95 per cent confidence level, and $NVA>0$) at least 90 per cent of the time. The DV is quoted as the ratio of the standard deviation of the noise-free flux variations to the mean count rate of the light curve, expressed as a percentage.

To determine the DV for each light curve in the sample, 25 different light curves, all with the same properties of length, temporal structure, mean count rate and photon-counting noise level as the observed light curve, were simulated using the methods outlined in Section 2.2. The standard deviation of the noise-free flux variations was once again calculated as a percentage of the mean count rate as above. The standard analysis (as outlined in Section 2.1) was then carried out on these light curves and from the results of this analysis a probability of the detection of variability was calculated. This process was repeated for noise-free flux variations of different amplitudes, and it was then trivial to find the amplitude of noise-free flux variations at which variability was detected on at least 90 per cent of occasions. The DV for each light curve is then given the value of the standard deviation of the noise-free flux variations expressed as a percentage of the mean flux of the light curve.

This definition of DV means that the *lower* the DV for any light curve, the *higher* the probability of detecting flux variability. The effects of differing sensitivity to the detection of variability are investigated further in Section 3.3.1.

2.5 Simulations to determine the errors on the power spectrum parameters

Due to the use of CLEAN to remove the effects of the window function, the errors on the power spectrum parameters must be deduced via simulations.

For the purposes of determining the errors on the power spectrum parameters, 80 light curves were simulated with the same power spectrum slope, temporal structure, mean count rate and standard deviation as each original observed light curve. The standard deviation of the intrinsic source variability ($\sigma_{\rm signal}$) was deduced from the equation

$$\sigma^2_{\rm total} = \sigma^2_{\rm noise} + \sigma^2_{\rm signal}, \qquad (3)$$

where $\sigma_{\rm total}$ is the standard deviation of the light curve, $\sigma_{\rm noise}$ is the standard deviation of the photon-counting noise, which is calculated simply from the total number of photons in each time bin, and $\sigma_{\rm signal}$ is the standard deviation of the intrinsic source variability. From the spread in the measured power spectrum slope and normalization of the power spectra of 80 simulated light curves an error was deduced for these parameters.

To gauge the accuracy of the method used here we compare the value thus obtained for the power spectrum slope of the 200-ks 1986 observation of MCG-6-30-15 with the value obtained using the more accurate but more computer-intensive method of Done et al. (1992) and Fiore et al. (1993). In the latter method many light curves with similar temporal structure to the observed light curve and a variety of theoretical power spectrum slopes are simulated and their power spectra are generated. These simulated power spectra are then compared with the observed power spectra. This method does not involve the use of the CLEAN algorithm. Using our method we obtain a value for the power spectrum slope of $-1.36^{+0.26}_{-0.32}$ (1σ errors), whereas that obtained using the Done et al. method is $-1.28^{+0.12}_{-0.19}$ (1σ errors). These two results agree well, showing that our method produces accurate results. A significant drawback in the Done et al. method appears to be that only slopes flatter than $\alpha=-1.6$ can be measured (Fiore et al. 1993) due to the problems caused by the window function for slopes ≤ -2 (see Section 2.1). Our method is also much less computer-intensive than the Done et al. method.

For our sources we have assumed that the power spectrum will be well fitted by a simple power-law and noise model. The obvious exception to this assumption is the source NGC 6814 which has a well-known periodicity with a period of 12132 ± 3 s (Done et al. 1992). For NGC 6814 we therefore ignore the frequencies around 8×10^{-5} Hz in the fitting of the power-law model.

For MCG-6-30-15 it is possible to test whether a simple power-law model is a good fit to the data. Using the method of Done et al. (1992) it is possible to obtain a value for the χ^2 statistic of the best-fitting model. In the case of MCG-6-30-15 the best-fitting χ^2 statistic is 12.1 with 19 degrees of freedom, which implies that the simple power-law model is a good fit to this power spectrum.

Fig. 1 shows the binned power spectrum for the 1986 observation of MCG-6-30-15. Fig. 1(a) shows the power

Table 1. Log of all observations used.

Source Name	Obs Date	Count Rate (cts/sec)	Obs Length (ksec)	variable (yes/no)	Luminosity (logarithmic) (see text)	detectable variability %
MKN 335	84/341	1.28	33.5	N	43.64	32.2
MKN 335	85/334	1.35	28.1	N	43.64	> 33.0
III ZW2	85/354	2.75	24.4	N	45.10	15.6
III ZW2	85/199	2.27	24.3	N	45.00	23.0
FAIRALL-9	85/207	1.76	20.8	N	44.32	22.9
NGC 526	83/249	2.27	24.1	N	43.75	22.3
MKN 1040	84/259	1.52	20.2	N	43.37	28.9
0241+622	83/350	3.69	24.0	N	44.62	11.1
0241+622	83/245	2.93	20.4	N	44.53	16.1
3C 120	84/276	4.11	44.5	Y	44.42	12.4
3C 120	84/280	3.27	25.5	N	44.31	12.6
3C 120	84/249	3.99	30.7	N	44.38	12.8
3C 120	84/277	3.59	23.6	N	44.35	13.1
3C 120	84/278	3.64	21.5	Y	44.38	15.8
3C 120	84/284	3.05	20.8	N	44.26	16.4
3C 120	83/305	2.89	22.9	N	44.19	16.5
3C 120	83/228	3.18	44.5	N	44.31	19.8
3C 120	85/283	3.70	53.4	N	44.36	24.1
3C 120	86/044	2.29	22.8	N	44.14	24.1
3C 120	86/031	2.78	26.2	N	44.30	> 33.0
AKN 120	85/024	3.37	23.9	N	44.29	13.0
NGC 2110	84/310	1.71	23.0	N	42.77	> 33.0
MCG+8-11-11	85/308	5.47	26.3	Y	44.08	11.4
MCG+8-11-11	86/040	4.55	27.8	Y	44.03	11.4
MCG+8-11-11	85/282	3.52	27.2	N	43.90	15.2
3A0557-383	84/350	2.32	28.0	N	43.86	> 33.0
NGC 2992	83/352	2.44	25.8	N	42.96	17.4
NGC 2992	84/344	2.99	20.5	N	43.05	18.0
NGC 2992	84/096	1.27	32.0	N	42.72	23.0
NGC 3227	85/342	4.14	23.4	Y	42.56	12.3
NGC 3227	83/349	3.78	21.9	Y	42.49	19.0
NGC 3227	85/349	2.39	29.1	Y	42.33	21.1
NGC 3227	85/329	2.18	27.5	N	42.30	22.8
NGC 3516	85/311	1.27	39.5	N	42.80	28.9
NGC 3516	85/308	1.37	37.5	N	42.80	> 33.0
NGC 3783	84/162	6.14	23.9	Y	43.62	9.13
NGC 3783	85/005	4.21	24.8	N	43.42	12.0
NGC 3783	83/347	3.22	29.8	N	43.35	16.3
NGC 3783	85/053	3.85	23.3	N	43.38	18.9
NGC 4051	85/337	1.79	207.6	Y	41.73	15.2
NGC 4051	84/099	1.96	34.2	Y	41.67	29.7
NGC 4151	85/002	21.05	28.5	Y	43.19	3.00
NGC 4151	84/357	16.48	20.1	Y	43.10	4.75
NGC 4151	85/135	9.56	35.7	Y	42.87	5.90
NGC 4151	83/192	8.57	143.6	Y	42.87	6.04
NGC 4151	85/118	5.99	22.8	N	42.68	8.55
NGC 4151	83/351	5.75	26.3	N	42.65	8.90
NGC 4151	86/060	5.72	124.7	Y	42.66	9.00
NGC 4151	83/319	3.89	23.7	N	42.48	10.7
NGC 4151	85/111	3.66	22.3	N	42.47	11.8
NGC 4151	83/311	5.62	26.4	Y	42.69	12.4
NGC 4151	84/109	2.20	28.8	N	42.22	19.0
NGC 4151	84/098	2.32	26.8	N	42.27	21.4
3C 273	86/017	8.78	145.1	Y	46.14	3.13
3C 273	83/351	13.58	29.5	N	46.32	5.38
3C 273	84/006	7.21	39.8	N	46.04	6.27
3C 273	84/136	6.70	27.7	N	46.11	6.60
3C 273	84/180	7.18	41.0	N	46.04	6.60
3C 273	85/032	6.24	23.5	Y	46.00	6.61
3C 273	85/138	8.65	40.7	N	46.00	6.33
NGC 4593	84/183	3.53	23.7	Y	43.17	14.1
NGC 4593	86/009	2.67	95.6	Y	43.05	14.1
NGC 4593	84/154	2.92	21.7	N	43.07	15.3
NGC 4593	85/185	1.49	36.1	N	42.79	26.3
NGC 4593	85/180	1.40	23.4	N	42.75	31.8
CENTAURUS-A	84/044	11.19	44.2	N	42.47	4.11
CENTAURUS-A	84/160	7.56	31.7	N	42.33	6.04
CENTAURUS-A	84/211	8.45	37.1	N	42.31	6.18
MCG-6-30-15	86/029	3.99	183.6	Y	43.05	6.57
MCG-6-30-15	84/202	3.07	29.4	Y	43.00	15.6
IC4329	84/201	12.30	22.9	N	44.25	6.56
IC4329	85/212	8.55	34.2	N	44.09	8.08
NGC 5506	86/024	6.96	256.0	Y	43.20	5.13
NGC 5506	84/061	6.44	23.3	Y	43.10	8.08
NGC 5506	85/032	7.41	24.4	Y	43.24	9.80
NGC 5506	85/041	6.39	22.7	Y	43.18	12.2
NGC 5506	85/053	4.88	27.9	Y	43.09	12.4
NGC 5506	83/235	4.79	29.2	Y	43.05	12.8
NGC 5548	86/019	5.27	63.7	N	43.92	6.39
NGC 5548	84/062	4.64	33.7	N	43.83	9.75
NGC 5548	84/193	3.11	64.5	N	43.67	12.8
NGC 5548	85/062	3.80	27.7	N	43.77	13.1
NGC 5548	85/186	2.00	24.4	N	43.55	22.0
NGC 5548	85/195	1.52	20.2	N	43.39	29.5
E1821+643	85/160	1.56	22.3	N	45.90	26.4
E1821+643	85/223	1.61	23.8	N	45.92	30.7
E1821+643	85/280	1.60	21.2	N	45.94	> 33.0
E1821+643	85/296	1.61	23.4	N	45.94	> 33.0
3C 382	85/246	3.72	22.8	N	44.85	13.0
3C 382	85/161	3.02	24.9	N	44.74	16.1
3C 382	85/256	3.34	23.5	N	44.81	17.8
3C 382	85/211	2.85	43.0	N	44.75	25.5
3C 382	85/117	1.93	20.1	N	44.55	26.1
3C 382	85/102	1.50	20.1	Y	44.56	27.4
3C 390	86/076	1.67	31.0	N	44.49	26.4
3C 390	85/033	2.17	55.8	N	44.61	30.7
NGC 6814	85/289	1.80	101.9	Y	42.47	19.7
NGC 6814	83/306	1.65	30.0	Y	42.42	21.9
NGC 6814	84/287	1.35	23.3	Y	42.29	24.1
NGC 6814	83/247	2.55	20.4	Y	42.60	25.8
NGC 7314	84/315	2.99	22.5	Y	42.55	13.1
MR 2251-179	83/279	2.44	91.6	N	44.80	13.2
MR 2251-179	84/325	2.36	21.4	N	44.83	21.1
MR 2251-179	84/332	2.13	23.5	N	44.77	22.2
MR 2251-179	84/316	1.75	27.7	N	44.68	22.6
MR 2251-179	84/307	1.60	23.7	N	44.66	27.8
MR 2251-179	83/300	1.50	21.2	N	44.63	29.5
MR 2251-179	84/292	1.40	30.7	N	44.61	31.8
NGC 7469	84/332	2.83	26.4	N	43.60	16.1
MCG 2-58-22	84/321	2.46	23.3	N	43.89	19.0

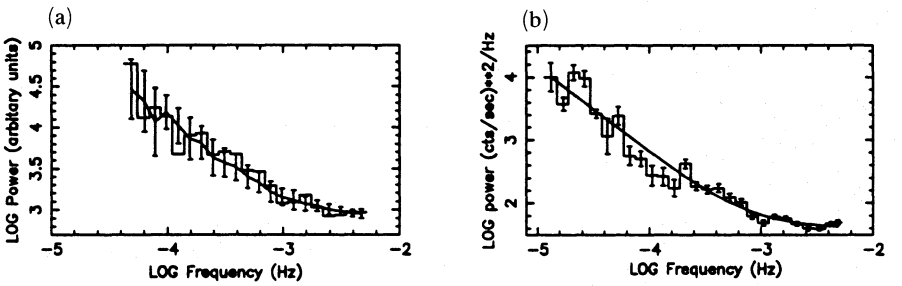

Figure 1. (a) Power spectrum for MCG-6-30-15 using the Done et al. method as outlined in Section 2.5. The error bars here are true error bars, derived from simulations. The power spectrum has not been CLEANed as the model is also UNCLEANed. (b) CLEANed power spectrum together with model fit to the data. The error bars here simply represent the scatter in the original unbinned data points, as described in Section 2.1.

spectrum of MCG-6-30-15 as a histogram, and the best-fitting power spectrum as found using the method of Done et al. as a continuous line. The error bars are the 1σ errors deduced from the simulations. Fig. 1(b) shows the CLEANed power spectrum for MCG-6-30-15 (histogram) together with the best-fitting model found using the method described in Section 2.1.

As we have the power spectra for the 80 simulated light curves we can find the expected spread in the value for the power in the observed power spectrum from the standard deviation of the spread in the simulated spectra. This is similar to the method by which errors are calculated by Done et al. We find that all the power spectra are consistent with the simple power-law model.

3 ANALYSIS OF SOURCES

The *standard analysis* outlined in Section 2 was performed on all 110 light curves that satisfied the selection criterion. Of these 110 light curves a total of 34 proved to be variable. Even though these light curves satisfied the statistical requirements for variability, all the light curves were visually checked, as poor background-subtraction can lead to a systematic difference in observed flux, for a constant source, between observations from the two different halves of the ME instrument. In cases where this systematic difference was found, its value was estimated and half of the value was added to the data obtained from one half of the ME instrument, and subtracted from data obtained with the other half, in such a way as to remove the systematic offset. The light curve was then reanalysed for variability.

Table 1 lists all the light curves studied, together with their mean count rates, length of observation, luminosities, and whether variability was seen. Also listed in the table is the DV as defined in Section 2.4. Table 2 shows the details of the variability on a source-by-source basis. If the source is non-variable then the power spectrum slope is undefined and the *NVA* is given an upper limit derived from the observation with the lowest photon-counting noise in the power spectrum (for these sources no error is shown on the *NVA*). The errors shown on the power spectrum slope and *NVA* are 1σ errors obtained by using simulations, as described in Section 2.5. For the photon index the quoted errors are 90 per cent confidence limits. The grouping of the light curves to give the parameters for each source is discussed in more detail in Section 3.1. The DV shown in Table 2 is the DV of the light curve of best signal-to-noise ratio for that source.

It is possible that AGN with different *energy* spectra may have different variability characteristics. In order to search for any such effects we determined the energy spectra of our sample. Although some of the spectra have been previously published by other authors (e.g. Turner & Pounds 1989) we calculated all energy spectrum parameters ourselves in the same manner in order to retain continuity throughout the work. We derived the spectral parameters by fitting an absorbed power-law spectrum to the background-subtracted ME spectra extracted from the *EXOSAT* data base. Although this model is not necessarily the best-fitting model it does enable us to obtain a reasonable value for the power-law slope, flux, and hence luminosity, which can then be used in correlations. The column density is not used in the correlations as the ME spectral data are not of good enough quality to constrain this parameter well.

The luminosity was calculated in the 2–10 keV energy range using redshift data from the NASA Extragalactic Database (NED), an H_0 of 50 km s^{-1} Mpc^{-1} and a q_0 of 0.5. NED was also the source of the class of each object as given in Tables 2 and 3.

3.1 Is AGN variability a statistically stationary process?

With our sample (many light curves of the same source) it is possible to put some constraints on whether the variability process is statistically stationary. If the process were statistically non-stationary we would expect to see different power spectrum slopes and/or different amplitudes of variability when we observe a source at different epochs. We have to take into account, however, the fact that all the observations of a particular source give us light curves that have different signal-to-noise ratios, and hence different probabilities of detecting variability. In Table 1 the sources are ordered in right ascension, with the observations of each source being listed in order of decreasing sensitivity to the detection of variability. (Remember that this ranking depends on average source flux as well as on length of observation.) We can see that, in the cases where flux variability is not detected in all of the observations of a source, variability is generally detected in the observations with the lowest DV (i.e. the highest probability of detection of variability), and there is only one case (3C 382) where the source appears to show flux variability in the light curve with the highest DV.

As discussed in Section 2.3, if the light curve has a very high DV then the simulations show that it is possible that on some occasions the derived power spectra might actually

Table 2. Details of source variability – see text for full description.

Source Name	Source Class	Power Spectral Slope	*NVA*	Photon Index	LOG Luminosity erg s^{-1}	DV %
MKN 335	Sy 1		4.30	2.21 ± 0.13	43.64	32.2
III ZW2	Sy 1/QSO		2.90	1.73 ± 0.17	45.05	15.6
FAIRALL-9	Sy 1		3.30	1.88 ± 0.15	44.32	22.9
NGC 526	Sy 1.5		2.90	1.16 ± 0.17	43.75	22.3
MKN1040	Sy 1.2		3.50	1.64 ± 0.18	43.37	28.9
0241+622	Sy 1		2.90	1.70 ± 0.13	44.58	11.1
3C 120	Sy 1	$-2.20^{+0.67}_{-1.2}$	1.59 ± 0.82	1.79 ± 0.09	44.31	12.4
AKN 120	Sy 1		1.60	2.03 ± 0.13	44.29	13.0
NGC 2110	Sy 2		5.20	1.46 ± 0.43	42.77	>33.0
MCG 8-11-11	Sy 1		± 0.45 ± 0.16	1.76 ± 0.14	44.00	11.4
3A0557-383	Sy 1		1.80	2.51 ± 0.18	43.86	> 33.0
NGC 2992	Sy 2		2.00	1.41 ± 0.17	42.91	17.4
NGC 3227	Sy 2		1.27 ± 0.60	1.65 ± 0.06	42.42	12.3
NGC 3516	Sy 1		3.90	1.62 ± 0.17	42.80	28.9
NGC 3783	Sy 1	$-1.26^{+0.54}_{-1.0}$	1.59 ± 1.13	1.37 ± 0.06	43.44	9.13
NGC 4051	Sy 1	$-1.33^{+0.32}_{-0.45}$	5.78 ± 2.08	2.00 ± 0.13	41.70	15.2
NGC 4151	Sy 1	$-2.11^{+0.47}_{-0.62}$	0.76 ± 0.27	1.37 ± 0.16	42.68	3.00
3C 273	QSO	$-2.48^{+0.82}_{-0.76}$	0.20 ± 0.08	1.58 ± 0.03	46.09	3.13
NGC 4593	Sy 1	$-1.75^{+0.42}_{-0.64}$	3.13 ± 1.15	1.98 ± 0.18	42.97	14.1
CENTAURUS-A	R Gal		0.60	1.33 ± 0.11	42.37	4.11
MCG-6-30-15	Sy 1	$-1.36^{+0.25}_{-0.32}$	3.87 ± 0.92	2.03 ± 0.08	43.05	6.57
IC4329	Sy 1		0.70	1.70 ± 0.05	44.18	6.56
NGC 5506	Sy 1.9	$-2.05^{+0.28}_{-0.31}$	1.919 ± 0.35	1.92 ± 0.07	43.14	5.13
NGC 5548	Sy 1		1.30	1.53 ± 0.07	43.69	6.39
E1821+643	QSO		3.40	1.97 ± 0.33	45.92	26.4
3C 382	Sy 1		1.40	1.74 ± 0.19	44.71	13.8
3C 390	Sy 1		3.40	1.51 ± 0.19	44.55	26.4
NGC 6814	Sy 1	$-0.91^{+0.32}_{-0.58}$	4.79 ± 2.75	1.85 ± 0.18	42.44	19.7
NGC 7314	Sy 1		6.68 ± 2.56	1.95 ± 0.24	42.55	13.1
MR2251-179	QSO		2.40	1.81 ± 0.17	44.71	13.2
NGC 7469	Sy 1		2.00	1.70 ± 0.06	43.60	16.1
MCG2-58-22	Sy 1		2.30	1.67 ± 0.24	43.89	19.0

have non-zero *NVA*, even if there is no signal present. The observation of 3C 382 in which flux variability was detected was the observation with the highest DV, being only 20.1 ks in length and having a mean count rate of only 1.5 count s^{-1}. As this observation was so short and the source was in a low flux state it is likely that the detection of flux variability is spurious and hence the data are almost certainly consistent with a stationary process for the variability of 3C 382.

In the case of NGC 5506 there are a sufficient number of observations that we are able to examine whether variability is statistically stationary in some detail. Besides the 250-ks 'long look' (McHardy & Czerny 1987) there are five other *EXOSAT* observations of NGC 5506, and significant flux variability has been detected in all of these light curves. In four out of the six observations power spectra of reasonable quality can be obtained. The characteristics of the power spectra are calculated by the methods used in Section 2.1. The power spectrum slopes and *NVA*s are consistent with the average values quoted in Table 2 and derived from the 'long look' (see Section 3.2 for more detail about the power spectrum parameters derived from the 'long look' at this source). Thus all of the observations of NGC 5506 are consistent with the hypothesis that the variability in this source is statistically stationary.

We now re-examine the suggestion of Barr et al. (1987) that the flux variability observed in NGC 4593 may be non-statistically stationary. Barr et al. found that on day 185 of 1985 and day 9 of 1986 the power spectra of the flux variations in NGC 4593 were very similar, but on day 176 of 1985 the power spectrum still had the same slope but had a higher normalization, giving the appearance of a shift in the power spectrum to higher frequencies.

The observation of NGC 4593 on day 176 of 1985 does not meet the selection criteria for the present work as the mean count rate is only 1.1 count s^{-1}. However, as NGC 4593 is the only source for which the claim has been made that the flux variations are not statistically stationary, we analyse it none the less. The analysis that we have carried out shows that the quality of the power spectrum of the light curve is poor, and consequently it is not possible to say with any certainty that the power spectrum of the light curve taken on day 176 of 1985 is significantly different from the power spectra obtained from other observations of NGC 4593.

The results that, for a specific source, the light curves in which variability is detected are the light curves with the lowest DV, and that for NGC 5506 in particular the power spectrum slopes and *NVA*s are all consistent at different

epochs, lead us to conclude that we find no evidence that AGN variability is a statistically non-stationary process.

It should be pointed out, of course, that, until we achieve data of infinitely high signal-to-noise ratio and infinite duration, we cannot prove absolutely that variability in any source is statistically stationary. We would only be able to draw a definite conclusion if we found strong evidence against statistically stationary variability. However, as we have no evidence to the contrary, we assume that X-ray AGN variability is statistically stationary, and so from here on we group together all the light curves of each source to give the average properties of that source. Depending on the number of times variability is observed in each source, the grouping is carried out by one of three methods outlined below.

(i) If all of the observations are seen to be variable, the *NVA* and power spectrum slopes deduced from each observation of a source are combined to give a weighted mean value for that source.

(ii) If the source is not seen to be variable in any observation, the power spectrum slope is undefined, and the *NVA* is given as an upper limit deduced from the photon-counting noise levels of the lowest noise observation.

(iii) For some sources variability is detected in the light curves with the lowest DV but not in the light curves with a high DV. As these results are entirely consistent with the process being statistically stationary we take the value of the variability parameters (i.e. *NVA* and the power spectrum slope) from the light curves with the lowest DV and ignore the higher upper limits deduced from the poorer quality observations.

3.2 Breaks in the power spectra

The multiple shot-noise model described in Section 1 predicts two breaks in the power spectrum slope, one at high frequencies, above which the slope tends to -2, and a second at lower frequencies, below which the power spectrum flattens to a slope near zero. In this study, the calculated power spectra cover the frequency range 10^{-5} to 5×10^{-3} Hz, although the signal generally intercepts the noise at about 10^{-3} Hz. For nine sources we are able to calculate high-quality power spectra. In six out of the nine sources the power spectrum slope can only be measured over one decade of frequency, between $10^{-4.5}$ and $10^{-3.5}$ Hz, and so power spectrum breaks are unlikely to be seen. However, in the other three sources, NGC 4051, MCG-6-30-15 and NGC 5506, the power spectrum slope can be measured over two decades from 10^{-5} to 10^{-3} Hz. In these cases the power spectrum slopes were measured at frequencies higher than 10^{-4} Hz by fitting the power-law-plus-noise model. A power-law-plus-noise model, with the noise level fixed to be the same as that determined from the fit at frequencies above 10^{-4} Hz, was then fitted to the data in the region 10^{-4} to 10^{-5} Hz. For both NGC 4051 and MCG-6-30-15 the measured power spectrum slopes did not change significantly between the two frequency regions. However, for NGC 5506 the slope at high frequencies was -1.9 but the slope at lower frequencies was -1.4. The error on the high-frequency slope is about ±0.7 and the error on the low-frequency slope is about ±0.4, and so, although there is an indication here that the power spectrum slope of NGC 5506 steepens at higher frequencies, the two slopes are consistent with having the same value.

As NGC 5506 is the only source for which we have an indication of variation of power spectrum slope with frequency, we conclude that a simple power law provides a good description of the power spectrum, and measure its slope for all sources in the range $10^{-4.5}$ to $10^{-3.5}$ Hz. These values are quoted in Table 2.

3.3 Occurrence of variability

As can be seen from Table 2 variability is detected on at least one occasion in about one third (12 out of 32) of the sources. To explain why some sources have a larger amplitude of variability than others we have investigated the occurrence of variability in terms of the DV, source classification (i.e. Seyfert 1, QSO, etc.), X-ray luminosity and *energy* power-law index.

3.3.1 Observation length and mean flux level

We discussed in Section 2.3 the effects that the length of the observation and the mean flux of the source have on the probability of detection of variability and defined a quantity called the detectable variability (DV). The DV is specific to each light curve and gives a measure of the amplitude of the noise-free flux variations that we can expect to detect given a light curve of certain observation length, mean flux and photon-counting noise. In this section we show how the DV affects the probability of detection for this sample.

Figure 2 shows the cumulative total of sources (both the total number and the number of variable sources) as a function of the DV. It can clearly be seen that up to a DV of around 15 the ratio of variable to total sources remains fairly constant, but at DVs higher than 15 the curves start to diverge. For sources with DV$\leq$15, about 58 per cent of sources show short-term flux variability.

This cut-off in the number of sources seen to be variable at a particular DV suggests that the criteria for accepting light curves into our sample outlined in Section 2 were too liberal and could be tightened without loss of information. However, Fig. 2 also shows that we can be reasonably confident that we have selected all the light curves that may show variability.

3.3.2 Source class

Table 3 shows a breakdown of the occurrence of variability within different classes of AGN. As can be seen from this

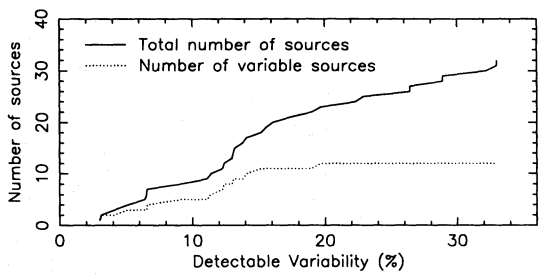

Figure 2. Cumulative number of sources as a function of detectable variability (DV).

table, with the possible exception of QSOs, the class of source does not seem to be a major factor when considering the occurrence of flux variability. The reason that fewer QSOs are seen to vary will become evident in the next section.

Table 3. Breakdown of sources by class.

source class	number of objects	number of variable objects	percentage of variable objects	average detectable variability
Seyfert 1	21	8	38	16.0
Other Seyferts	6	3	50	19.0
QSOs	4	1	25	14.6
Radio Galaxies	1	0	0	4.1

3.3.3 *Luminosity*

Fig. 3(a) shows a histogram of the total number of sources and number of variable sources in each logarithmic luminosity bin. Fig. 3(b) has been derived directly from Fig. 3(a) and shows the percentage of variable sources per luminosity bin, and Fig. 3(c) shows the average DV per luminosity bin, with the average DV for the whole sample being shown as the dashed line.

There appears to be a trend in Fig. 3(b) for the percentage of variable sources to decrease as the luminosity increases. This trend seems quite strong, with the exception of the highest luminosity bin. The highest luminosity bin contains only one source, 3C 273, which as can be seen from Fig. 3(c) has a very low DV (i.e. a very high probability of detection). Of the seven observations of this source, variability was detected in only two (see Table 1), even though the average DV over all seven light curves is only 5.8 (the average for the whole sample is 16.11). If the DV for 3C 273 is 16.11 it is likely that no variability would have been detected, hence strengthening the apparent trend.

It could be said that the trend also relies heavily on the lowest luminosity bin which contains only one source. The source in this bin is NGC 4051 which was observed on two occasions with DVs of 15.2 and 29.7. On both occasions the source was seen to vary dramatically and as the DVs are of the order of the mean value or higher we cannot say that this point is atypical.

3.3.4 *Energy spectrum*

The histogram in Fig. 4(a) shows the distribution of photon indices derived from the spectral fits for all the sources in the sample and for only the variable sources in the sample. Fig. 4(b) is derived directly from Fig. 4(a) and shows the percent-

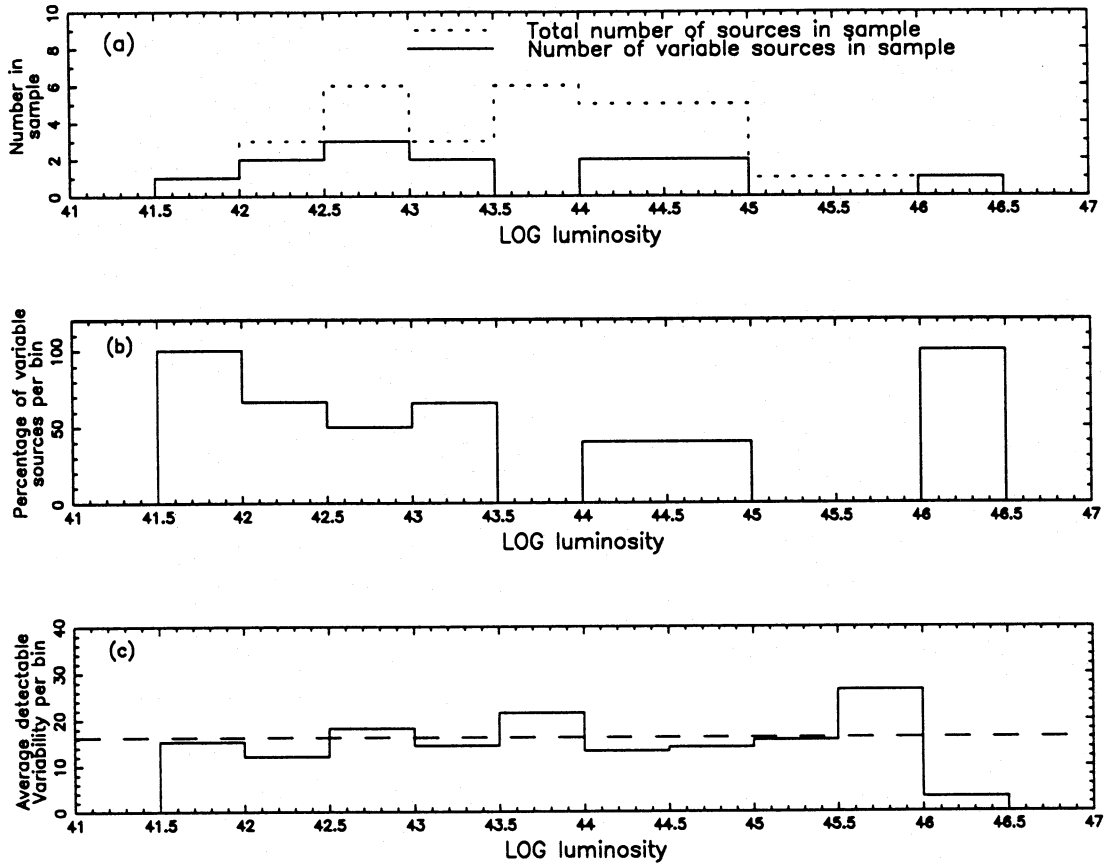

Figure 3. (a) Distribution of the luminosity of sources in the sample. (b) Percentage of variable sources per luminosity bin derived directly from (a). (c) Average detectable variability per luminosity bin.

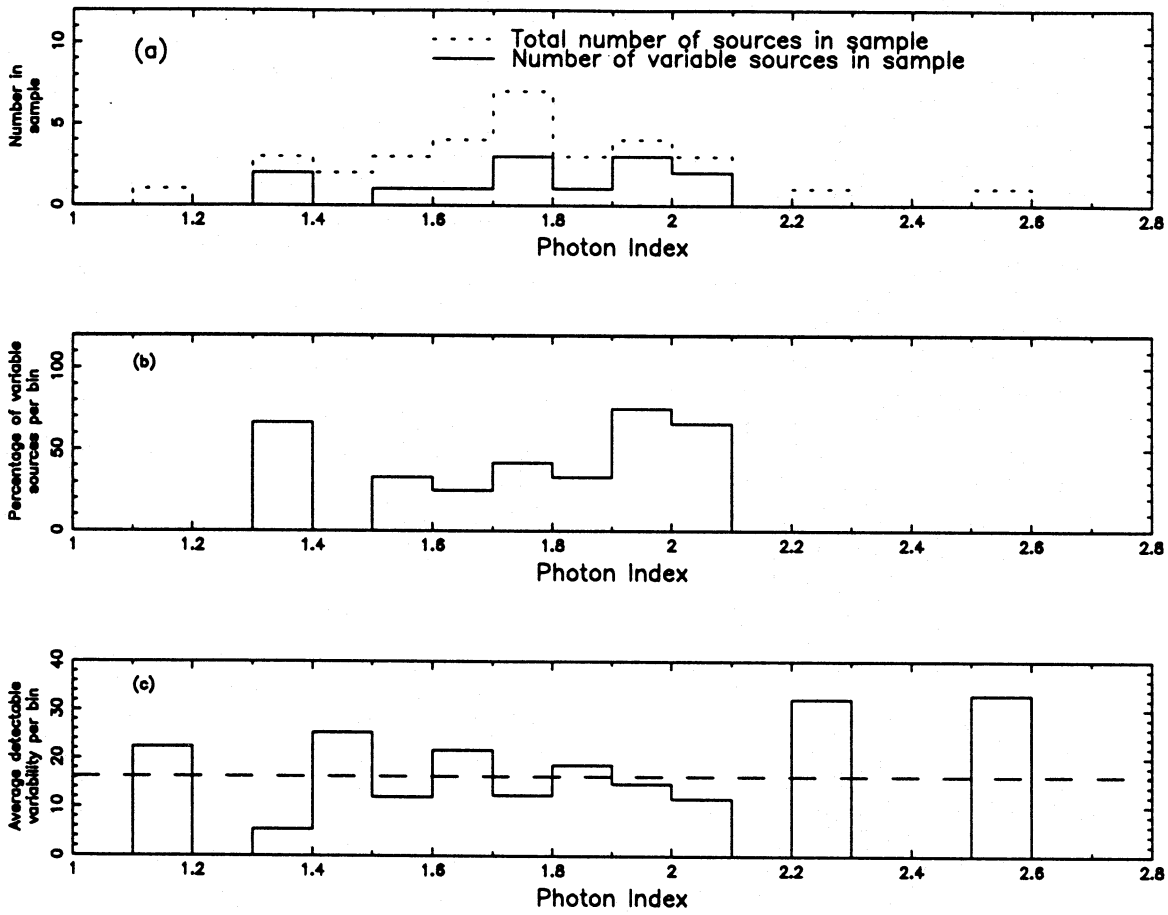

Figure 4. (a) Total number and number of variable sources as a function of photon index. (b) Percentage of variable sources as a function of photon index derived directly from (a). (c) Histogram showing the average detectable variability for each photon index bin, the dashed line representing the average DV for the whole sample.

age of sources seen to vary in each photon index bin, and Fig. 4(c) shows the average DV for each bin with the average DV for the whole sample being shown as a dashed line.

Fig. 4(b) shows a trend for the spectrally softer sources (i.e. steeper energy spectrum) to be seen to vary more often than harder sources. Once more, as above, it is necessary to look at the average DV which shows that the bin containing 3C 273 is atypical in having a very low DV, and hence a higher probability of detection of variability. Variability is not detected in the two sources with the steepest spectra, which apparently contradicts the observed trend, but Fig. 4(c) shows us that these two sources have a very low probability of detection (a high DV) and hence are still consistent with the observed trend.

3.4 The nature of the variability

The results of the previous section imply that spectrally softer sources and less luminous sources vary more often than harder sources and more luminous sources. We now investigate the nature of the variability seen in these objects by looking at their power spectrum slopes and *NVA* s.

3.4.1 *Correlations with the X-ray luminosity*

Figs 5(a) and (b) show how the power spectrum slope is related to the luminosity, with Fig. 5(a) showing individual data points and Fig. 5(b) showing these data points binned up into a histogram. It is not possible to obtain any limits on the power spectrum slope for the sources in which variability is not detected, hence none is plotted. The error bars represent the 1σ errors as deduced from the simulations described in Section 2.5. Figs 5(c) and (d) show the relationship between *NVA* and luminosity. Fig. 5(e) shows the *NVA* plotted versus luminosity in logarithmic space.

The power spectrum slopes are consistent with a mean value of -1.72 ± 0.52, although there is a hint that the higher luminosity sources have steeper power spectrum slopes (Fig. 5a shows the least-squares best fit to the data). The Spearman correlation test finds an inverse correlation significant at the >90 per cent confidence level, but if we remove the data point for 3C 273 the significance of the trend falls to only 75 per cent.

Fig. 5(a) shows the *NVA* as a function of luminosity. The upper limits are also plotted, and with one exception

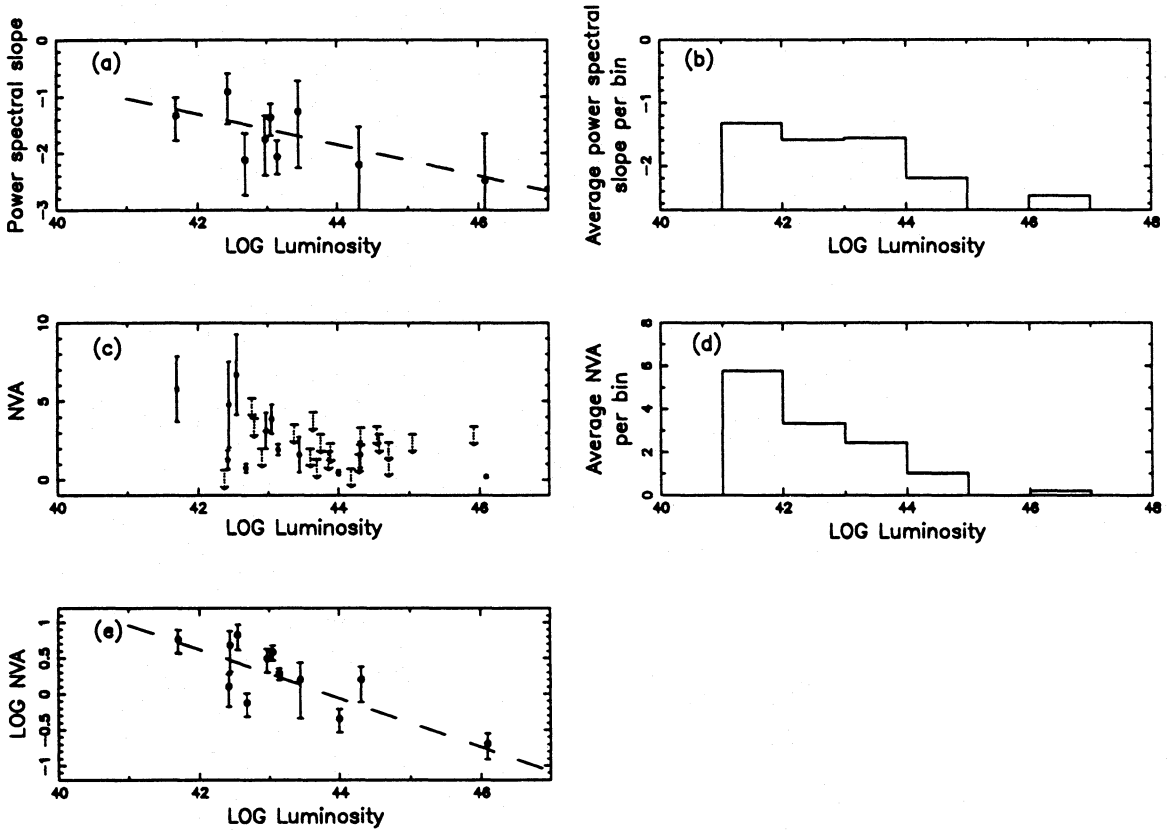

Figure 5. (a) ME power spectrum slope versus luminosity for the variable sources in the sample including a least-squares fit to the data. (b) Average power spectrum slope per luminosity bin. (c) *NVA* as a function of luminosity including upper limits for sources that are not seen to vary. (d) Average *NVA* per luminosity bin. (e) Log *NVA* versus log luminosity showing a least-squares fit to the data.

(Centaurus A) are consistent with the trend that as luminosity increases the *NVA* decreases. The hypothesis that the *NVA* is constant for the whole sample is rejected at the >99.5 per cent confidence level using the χ^2 test. The trend seen in the data is once again confirmed with the Spearman correlation test and is found to be significant at the >95 per cent confidence level, and even without the data for 3C 273 there is still a correlation at the >90 per cent confidence level. In Section 4.4 we find that the X-ray emission from 3C 273 is not typical of the rest of the sample, probably due to a relativistically beamed component being present, and it is for this reason that the data for 3C 273 can be excluded from the plots.

Fig. 5(e) shows the *NVA* and luminosity plotted in logarithmic space together with the best-fitting line. This yields the relationship

$$NVA = 10^{14.9\pm2.6} \times L_{x(2\text{-}10\,\mathrm{keV})}^{-0.34(\pm0.06)}. \quad (4)$$

This trend qualitatively agrees with that found by both McHardy (1988) and Barr & Mushotzky (1986). The first paper used *EXOSAT* data and analysis methods very similar to those used here, but the second used data from a number of X-ray missions, implying that this is a trend associated with the sources and not just the data.

This trend can be explained by the hypothesis that higher luminosity sources are larger than lower luminosity sources if we assume that the overall emission regions are rather fragmented and inhomogeneous. Thus some parts of the emission region might brighten on some occasions, whilst others would fade. In a large source, which might be equivalent to a larger number (say N) of smaller sources, the chances of the whole emission region brightening at the same time would be much less than for one small source. Thus one might crudely relate N to L_x and hence expect $NVA \propto 1/\sqrt{N}$ or $NVA \propto L_x^{-0.5}$. However, if, as seems more physically realistic, the emission regions are not entirely independent, but are slightly correlated, then we expect larger changes in luminosity than simply $\sqrt{N}$ variations and hence $NVA \propto L_x^{-\alpha}$, where α is now less than 0.5.

3.4.2 *Energy spectrum*

Fig. 6(a) shows the power spectrum slopes for variable sources plotted against the photon index, with Fig. 6(b) showing a histogram of the same data. Figs 6(c) and (d) show the *NVA* plotted against the photon index, with Fig. 6(e) showing the *NVA* plotted versus the photon index in logarithmic space. Fig. 6(f) shows the photon index versus the luminosity for the sources in our sample.

There is no correlation between the photon index and the power spectrum slope, but there appears to be a correlation (shown in Figs 6c–e) between the *NVA* and the photon index. The result that the photon index and *NVA* are correlated

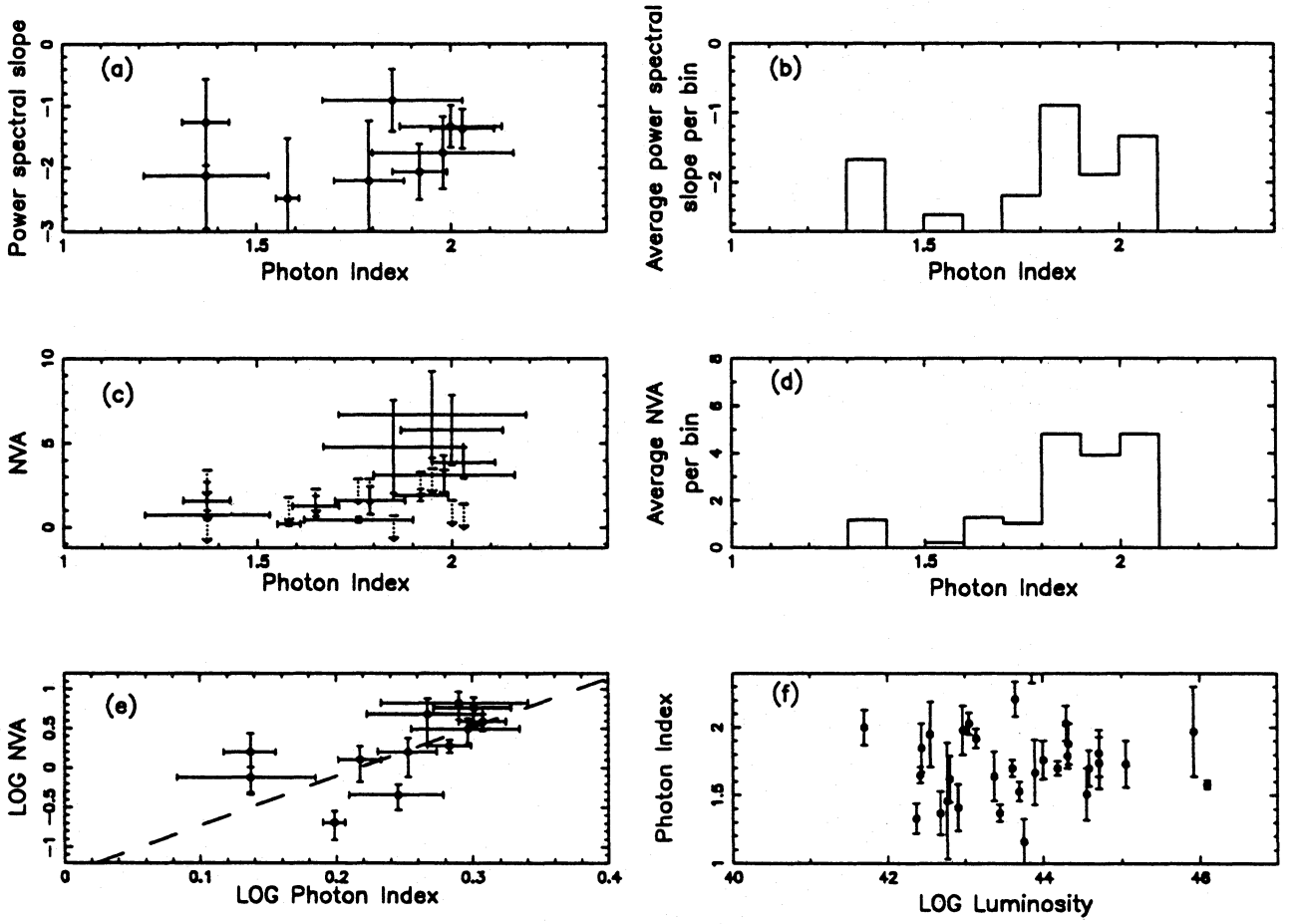

Figure 6. (a) Power spectrum slope versus photon index. (b) Average power spectrum slope per photon index bin. (c) *NVA* versus photon index. (d) Average *NVA* per photon index bin. (e) Log *NVA* versus log photon index showing a least-squares fit. (f) Photon index versus luminosity showing no apparent correlation, in agreement with Turner & Pounds (1989).

is somewhat weakened by the upper limits derived from the non-variable sources in the sample. However, of the nine sources in the sample with photon indices greater than 1.9, five show large-amplitude flux variations, and of the four remaining sources, two have very high DVs and one is a high-luminosity quasar, and we have already seen that the intrinsic variability for a high-luminosity object is low. The correlation between *NVA* and the photon index is found to be significant at the >99 per cent confidence level using the Spearman correlation test and is still found to be significant at the >98 per cent confidence level even when 3C 273 is removed from the data.

The relationship can be expressed by the equation

$$NVA = 0.05(\pm 0.03)\,\Gamma^{6.2(\pm 1.3)}. \quad (5)$$

At the present time the coefficients in this equation have no physical interpretation, but we hope that in the future models will be constructed that will account for this behaviour and make use of the values derived here.

Fig. 6(f) shows the luminosity plotted against the photon index for our sample. In agreement with the results found in Turner & Pounds (1989) for a slightly different sample, there is no trend evident in the data, showing that the correlation between *NVA* and the photon index is not an artefact of the correlation between *NVA* and luminosity.

In Section 4.1 the observed trend for softer sources to be more variable is explained in terms of the reflection model described in Pounds et al. (1990). It is known that little or no reflection occurs in the source NGC 4151 (Yaqoob 1992), so we should also exclude the data point for this source when looking for correlations. With the removal of the data point for NGC 4151 the trend is significant at the >95 per cent confidence level. The removal of data relating to NGC 4151 and 3C 273 does not alter the fit significantly. (The exponent changes from 6.2 ± 1.3 to 6.4 ± 1.9.)

3.5 The *EXOSAT* LE data

This paper is oriented towards data taken with the medium-energy experiment on *EXOSAT* rather than towards data taken with the low-energy telescope because in many cases the low-energy flux is heavily attenuated by absorbing material and so the number of 'good quality' LE light curves is very small.

However, two of the sources in our ME-selected sample, NGC 4051 and MCG-6-30-15, are bright enough low-energy sources that we are able to quantify their low-energy variability and compare it with their medium-energy variability. We have measured the low-energy power spectrum slopes and *NVA*s of these two sources as well as looking at

the cross-correlation coefficient between the ME and LE fluxes as a function of time lag. The power spectrum slopes are given in Table 4 and show that, although for each source the ME and LE power spectrum slopes are consistent within errors, the LE slopes seem to be systematically steeper than the ME slopes; the significance of this result will be discussed in Section 4.1. The *NVA*s are also consistent within errors and there appear to be no systematic differences.

The ME/LE correlation functions have a peak at zero for both sources, but both are asymmetric. In the case of MCG-6-30-15 this asymmetry has already been reported by Pounds & Turner (1987) who removed an extrapolation the ME component from the LE light curve and recalculated the cross-correlation function. The resulting cross-correlation function has a peak at a few thousand seconds in the sense that the LE flux changes are leading the ME flux changes.

For NGC 4051 the asymmetry in the cross-correlation function is less pronounced than, but is in the same direction as, for MCG-6-30-15. The spectral variability of NGC 4051 will be discussed in more detail in a future paper (M^{c}Hardy et al., in preparation).

4 DISCUSSION

4.1 Summary of results

We have systematically analysed 110 ME *EXOSAT* light curves of 32 AGN in an attempt to quantify the nature of flux variability in AGN. We list below the main findings of this work.

(1) Of the 32 sources in our sample, 12 sources exhibited detectable flux variability on at least one occasion.

(2) The *NVA* is approximately proportional to $L_x^{-1/3}$.

(3) Sources with steeper *energy* spectra have a higher *NVA*.

We additionally find, at a lower significance, the following.

(4) Although the data are consistent with a single value for the power spectrum slope for all sources, there is an indication that the power spectrum slope might be steeper for higher luminosity sources. In only one of the sources studied is there evidence of a possible change in the power spectrum slope with frequency.

(5) For the sources in our sample we find no evidence that flux variability is statistically non-stationary.

(6) For the small sample analysed, the power spectra of the LE light curves are systematically steeper than those of the corresponding ME light curves.

The implications of some of these observations have been discussed earlier in the paper, but we summarize them again here. In particular, we have shown how the inverse relationship between *NVA* and X-ray luminosity (point 2) can be explained naturally in a scenario where the overall emission comes from separate subregions of varying size which light up randomly, and where the size of the total emission region, and hence the number of subregions, is related to the black hole mass. The deviation of the data from the crude model applied in Section 3.4.1 is discussed in Section 4.2.

Table 4. Variability parameters of both LE and ME observations of NGC 4051 and MCG-6-30-15.

property	source	LE	ME
power spectral slope	NGC 4051	$-1.46^{+0.12}_{-0.20}$	$-1.33^{+0.32}_{-0.45}$
	MCG-6-30-15	$-1.59^{+0.12}_{-0.14}$	$-1.36^{+0.25}_{-0.32}$
NVA	NGC 4051	6.98 ± 0.83	5.78 ± 2.08
	MCG-6-30-15	2.77 ± 0.33	3.87 ± 0.92

One particularly interesting observation is that sources with steeper *energy* spectra have higher *NVA*s (point 3). This observation can be explained naturally in the context of reflection models as follows. Recent *Ginga* results (Pounds et al. 1990) have shown that the presence of cold material in, or near, the central regions of AGN can reprocess the hard X-ray radiation by reflection, thus producing a 'reflection hump' in the energy spectrum. This reflection hump appears between about 3 and 30 keV and hence, in the *EXOSAT* spectra, is unresolved and appears to flatten the energy spectrum. If a large amount of the original radiation is being reprocessed by reflection we would expect any rapid flux variations to be smoothed out by the reprocessing, and hence the amplitude of the flux variability we observe from outside the source would be significantly reduced. This reduction in the amplitude of flux variations will give rise to a reduction in the measured value of the *NVA*.

We have searched for evidence that X-ray variability might not be statistically stationary (point 5), as has been claimed in the case of NGC 4593 by Barr et al. (1987), but we find no evidence of statistically non-stationary behaviour in any of the sources in our sample. This presumably means that the emission mechanisms and approximate geometry do not change with time, but rather only the luminosity changes, perhaps responding to changes in the accretion rate.

There are a number of reasons why the LE power spectra might be steeper than the ME power spectra. The simplest reason is that the emission comes from completely different regions and is produced by different mechanisms. However, the similarity between the ME and LE light curves indicates a somewhat closer physical relationship between the regions emitting the LE and ME emission. It might be that the LE emission region is driven by the same unknown forces, such as random shocks, that power the ME region. However, it may lie further from the source of the shocks and the high-frequency shocks may have been damped out by passage through the ME region. Alternatively, both LE and ME emission may be produced in the same region but optical depth effects may reduce high-frequency activity in the LE band.

The above conclusions are largely independent of the model for the production of the X-ray emission. However, if we assume a particular emission model we are able to make further deductions. We thus proceed to examine our observations in the light of the variable decay shot-noise model (Lehto 1989a), and the rotating-spot model of Abramowicz et al. (1991).

4.2 'Variable decay shot-noise' or 'rotating-spot' model?

The variable decay shot-noise model (Lehto 1989a) proposes that the light curves are made up of a superposition of randomly separated shots of different amplitudes and with a power-law distribution of decay time-scales. At low fre-

quencies the power spectrum is flat and at high frequencies it has a slope of -2 with an intermediate slope at intermediate frequencies. The two breaks in the power spectrum correspond to the shots with the longest and shortest decay times. In the 'rotating-spot' model, hotspots on an accretion disc spiral around a black hole and relativistic beaming enhances the apparent flux from individual regions when they are moving towards the observer. Any variability intrinsic to the spot is also enhanced. The rotating-spot model (Abramowicz et al. 1991) predicts power spectra with a range of slopes depending on the variability intrinsic to the blobs of material, and the inclination of the disc. The model also predicts a decline in the power of the flux variations at frequencies related to the radius of the last stable orbit of matter spiralling into a black hole, which in turn is related to the black hole mass. (The cut-off time-scale scales linearly with black hole mass, and for a black hole mass of 10^7 $M_\odot$ is ~ 500 s).

As mentioned previously, the shot-noise model predicts that breaks should be observed in the power spectra of AGN. A break has possibly been observed in the power spectrum of NGC 5506, although the data are not of sufficient quality to provide any good constraints on the frequency at which the break occurs. McHardy (1988) presented the combined long- and short-time-scale power spectra for NGC 5506, which show that the power spectra also flatten at frequencies below $\sim$ few $\times 10^{-7}$ Hz. An analysis of data for 3C 382 (Kaastra 1991) shows that the power spectra of this source also flatten at low frequencies. The shot-noise model predicts a power spectrum shape very similar to that seen in the NGC 5506 data, but the rotating-spot model predicts that there might be a quasi-periodic structure at low frequencies (Abramowicz, private communication). It is clear that the power spectrum must turn over at low frequencies or the variance of the source fluctuations would be infinite, but a good knowledge of the precise shape of the power spectrum at low frequencies could separate the two models. The data we have at present cannot distinguish between the models.

In the shot-noise model neither the location of the regions emitting the shots nor the mechanism by which the emission is produced is specified. It has been suggested (McHardy 1988) that the shots may arise from subregions of an overall larger chaotic region which are temporarily lit up, perhaps by shocks. It is reasonable to suppose that the electron density would not be uniform throughout this region, perhaps decreasing with distance from the central engine, and the different shock decay time-scales might be a reflection of different cooling time-scales. Alternatively, the shocks might arise from magnetic field reconnection on the surface of an accretion disc (e.g. Pudritz & Fahlman 1982; de Vries & Kuijpers 1989). The shots would again be localized to small subregions and the parameters of the shots would scale with the radius from the central black hole. In either case, if the emission arises from small but basically similar localized regions then we expect to see $NVA \propto L_x^{-0.5}$, but if the regions are not entirely independent we expect $NVA \propto L_x^{-\alpha}$ where $\alpha < 0.5$.

In the rotating-spot model the precise nature of the spots of material is not certain. Abramowicz et al. (1992) suggest that magnetic vortices and magnetic flux tubes may be the cause of any region of enhanced intensity on a disc. To obtain the low-frequency turnover in the power spectrum as observed in NGC 5506 and in 3C 382, Abramowicz suggests that the intensity of each spot may decrease exponentially with time, which makes this model similar to the shot-noise model discussed above. The correlation between *NVA* and luminosity can be explained using this model if the times when the spots brighten are semicorrelated, hence producing a distribution of N semi-independent small sources as postulated above.

4.3 Black hole masses

The rotating-spot model can explain the power spectrum slope well, but also predicts that the power should fall off at high frequencies. We have not observed any cut-off in the power spectrum and so we can calculate upper limits on the black hole mass using the equation

$$\frac{M_{\rm BH}}{M_\odot} = 1 \times 10^4 t_{\rm min}. \qquad (6)$$

This equation assumes that the X-rays originate from regions ≥ 5 Schwarzschild radii from the black hole and that most of the variability arises from a region larger than 5 Schwarzschild radii. The parameter $t_{\rm min}$ (in units of seconds) is the shortest observed time-scale on which variability is detected. We define the shortest time-scale for variability as the time-scale that corresponds to the frequency at which the power of the source fluctuations (kf^α in equation 1) intercepts the power of the fluctuations caused by photon-counting statistics (the constant C in equation 1). The time-scale at which this interception occurs can be deduced from the parameters of the model fit to the power spectrum, which has been described in Section 2.1, using the equation

$$t_{\rm min} = \left(\frac{C}{k}\right)^{-1/\alpha}. \qquad (7)$$

Calculation of $t_{\rm min}$ in this way gives a rather conservative estimate of the shortest observable time-scale (and hence a high limit on the black hole mass), and by visually inspecting the light curve a smaller value could be estimated for $t_{\rm min}$. However, we prefer to use the values of $t_{\rm min}$ calculated from the power spectrum because they are not based on one-off flares which may be uncharacteristic of the general behaviour of the source.

We have deduced an upper limit on the black hole mass ($M_{\rm BH}$) for each source in which flux variability is detected, and these are shown in Table 5. The Eddington luminosities ($L_{\rm Edd}$) referred to in the last column are based on these masses.

Thus, if the rotating-spot model is correct, we deduce that central black hole masses are typically less than 10^8 $M_\odot$, but the present data are insufficient to show any correlation between L_x and $M_{\rm BH}$. For comparison we note that Dressler & Richstone (1990) calculated an upper limit on the black hole mass of 10^9 $M_\odot$ for M87 using stellar kinematics measurements, and that Pounds et al. (1987) deduced an upper limit of 10^7 $M_\odot$ on the black hole mass in Mrk 335 on the basis of X-ray spectrum considerations. These results are consistent with our deductions. We also note that, as the 2–10 keV luminosity that we list is a lower limit to the bolometric luminosity, the sources listed above are almost all radiating at a few per cent of their Eddington luminosities, and so pair production is likely to have some effect on the

Table 5. Calculated black hole masses assuming the rotating-spot model.

Source Name	LOG t_{min} (seconds)	lower limit on η	Upper limit on M_{BH} ($M_\odot$)	LOG $L_{x(2-10keV)}$ (erg s^{-1})	$L_{x(2-10keV)}/L_{Edd}$ $\times 10^{-3}$
NGC 3783	3.33	3.82×10^{-4}	2.2×10^{7}	43.44	9.9
NGC 4051	3.38	8.26×10^{-6}	2.4×10^{7}	41.70	0.16
NGC 4151	4.00	1.03×10^{-5}	1.0×10^{8}	42.68	0.37
3C 273	4.16	8.58×10^{-3}	1.5×10^{8}	46.09	650
NGC 4593	3.59	9.63×10^{-5}	3.9×10^{7}	42.97	1.8
MCG-6-30-15	3.14	1.51×10^{-4}	1.4×10^{7}	43.05	6.4
NGC 5506	3.47	5.00×10^{-5}	2.9×10^{7}	43.14	3.6
NGC 6814	3.43	5.84×10^{-5}	2.7×10^{7}	42.44	0.80

observed X-ray spectrum (e.g. Svensson 1987; Done, Ghisellini & Fabian 1990). The view that pair production is important in most AGN is also supported by the measurements of the compactness parameter as determined by Done & Fabian (1989).

In the variable decay shot-noise model there is no simple way to constrain the central black hole mass, although similarity in the overall (long- and short-time-scale) power spectrum of NGC 5506 with that of galactic black hole candidates such as Cyg X-1 has led to the suggestion (M^{c}Hardy 1988) that the frequency of the low-frequency break, or 'knee', in the power spectrum may scale with black hole mass, again leading to low black hole masses.

We can also derive the efficiency with which mass is converted to energy using measurements of dL_x/dt taken directly from the power spectrum. The efficiency parameter (η) is given by

$$\eta = 5 \times 10^{-43} \frac{dL_{bol}}{dt} \qquad (8)$$

(see Cavallo & Rees 1978; Fabian 1979). If we assume that the 2–10 keV X-ray luminosity is an underestimate of the bolometric luminosity by a factor of 10 or more then we can use values of dL_x/dt to determine η. Table 5 also shows the derived values for η. For all the sources except 3C 273 the values of dL_x/dt are less than 7×10^{37} erg s^{-1}, implying efficiencies of less than 3×10^{-4}. As the power spectrum slopes are all flatter than -2, measurements of dL/dt on shorter time-scales will lead to higher values of dL/dt and hence the efficiencies quoted here are lower limits.

3C 273 has an X-ray luminosity of 1.2×10^{46} erg s^{-1} and an upper limit to the black hole mass (derived from the power spectrum parameters in the rotating-spot model) of 1.5×10^{8} M$_\odot$. This upper limit on the black hole mass gives an upper limit on the Eddington luminosity of 2×10^{46} erg s^{-1}. As the apparent bolometric luminosity of 3C 273 is significantly greater than 4×10^{46} erg s^{-1} (see e.g. Hermsen et al. 1992), relativistic beaming effects are very probably occurring in 3C 273, a conclusion entirely consistent with observations of superluminal motion of radio components (e.g. Unwin et al. 1985) and observations of an X-ray jet in 3C 273 (Harris & Stern 1987).

4.4 Are black hole models essential?

Throughout this paper we have assumed that the energy required to power an AGN comes from either accretion processes on to a black hole or from the release of stored rotational energy from a black hole. There are, however, models of AGN that do not involve black holes, the most widely publicized of these being the starburst model (e.g. Terlevich et al. 1992).

In the starburst model the energy is generated by violent star formation activity in the innermost regions of AGN. The observed flux variability of AGN is ascribed to transient phenomena associated with the evolution of massive stars and supernovae. There is no difficulty in accounting for the average bolometric luminosity of AGN in terms of supernovae, but there is difficulty in accounting for it in terms of QSOs. For example, a Seyfert galaxy luminosity of 10^{44} erg s^{-1} can be accommodated by ~ 1 supernova per year [the energy released by one supernova (ignoring the neutrinos) being $\sim 10^{51}$ erg], whereas a rate of a few hundred supernovae per year is required for a high-luminosity QSO. With some ingenuity (e.g. Terlevich 1990) it is also possible to account for the observed spectra. However, we do not see how it is possible to account for the rapid X-ray variability discussed here and by other authors [e.g. the doubling of the luminosity from NGC 6814 in 50 s detected by Kunieda et al. (1990) with *Ginga*].

In most Seyfert galaxies, the energetic arguments stated above limit us to a supernova rate of a few per year. Thus we cannot attribute the continued short-time-scale large-amplitude rises and falls to the initial separate supernova explosions but have to link the variability with irregularities in an expanding blast wave. A few months after the initial explosion the diameter of the blast wave will typically be a few light days and so one would have to have an impossibly contrived density and space distribution of interstellar clouds to account for the observed continual variability on ~ 100-s time-scales. In addition, typical bremsstrahlung cooling time-scales are about 10^5 yr for typical interstellar densities and hence are far too long. The cooling time-scales would be reduced in dense molecular clouds, perhaps by factors of 10^4, but the cooling time-scales are still inconsistent with the observed variability. Finally, we note that, even if we could

somehow overcome these theoretical difficulties, *Ginga* observations of SN1987a (Arnett et al. 1989) show an X-ray light curve that rises slowly over a period of months rather than the sudden flares that are seen in AGN light curves.

4.5 Future work

This paper demonstrates the value of simple time-variability observations to our understanding of AGN. Here we have concentrated on *EXOSAT* observations of short-time-scale variability. Future papers will examine even shorter time-scale variability in the context of *ROSAT* and *Ginga* observations, and we will also discuss long-time-scale (~ decades) variability as deduced from archival data bases.

ACKNOWLEDGMENTS

The authors would like to thank the staff of the *EXOSAT* data base for their help and the NASA Extragalactic Database (NED) for information regarding redshifts and source class. ARG acknowledges receipt of an SERC studentship. Data reduction was carried out on the Southampton Starlink node.

NOTE ADDED IN PROOF

It has recently been discovered that the X-ray emission from NGC 6814 has been contaminated by a nearby Am Her type system (Madejski et al. 1993). On receiving this information, we have removed NGC 6814 from all our correlations and fits and we find no significant difference in any of the parameters we have derived.

REFERENCES

Abramowicz M. A., Bao G., Lanza A., Zhang X.-H., 1991, A&A, 245, 454
Abramowicz M. A., Lanza A., Spiegel E. A., Szuszkiewicz E., 1992, Nat, 356, 41
Albrecht M. A., Egret D., 1986, Databases and On-line Data in Astronomy. Kluwer, Dordrecht
Arnett W. D., Bahcall J. N., Kirshner R. P., Woosley S. E., 1989, ARA&A, 27, 629
Barr P., Mushotzky R. F., 1986, Nat, 320, 421
Barr P., Clavel J., Giommi P., Mushotzky R. F., Madejski G., 1987, in Treves A., ed., Variability of Galactic and Extragalactic X-ray Sources. Associazione per l'avanzamento dell'astronomia, Bologna, p. 43
Bregman J. N. et al., 1988, ApJ, 331, 746
Cavallo G., Rees M. J., 1978,, MNRAS, 183, 359
Deeming T. J., 1975, Ap&SS, 36, 137
de Vries M., Kuijpers J., 1989, in Hunt J., Battrick B., eds, Two Topics in X-ray Astronomy, ESA SP-296. ESA, Noordwijk, The Netherlands, p. 1069
Done C., Fabian A. C., 1989, MNRAS, 240, 81
Done C., Ghisellini G., Fabian A., 1990, MNRAS, 245, 1
Done C., Madejski G. M., Mushotzky R. F., Turner T. J., Koyama K., Kunieda H., 1992, ApJ, 400, 138
Dressler A., Richstone D. O., 1990, ApJ, 348, 120
Fabian A. C., 1979, Proc. R. Soc. Lond. A, 366, 449
Fiore F., Done C., Edelson R., Angelini L., 1993, ApJ, submitted
Giommi P., 1986, The EXOSAT Express, 12, 33
Giommi P., Barr P., Garilli B., Maccagni D., Pollock A. M. T., 1990, ApJ, 356, 432
Grandi P., Tagliaferri G., Giommi P., Barr P., Palumbo G. G. C., 1992, ApJS, 82, 93
Harris D. E., Stern C. P., 1987, ApJ, 313, 136
Hermson W. et al., 1992, A&AS, 97, 97
Högbom J., 1974, ApJS, 15, 417
Kaastra J. S., 1991, in Miller H. M., Wiita P. J., eds, Variability of Active Galactic Nuclei. Cambridge Univ. Press, Cambridge, p. 198
Kunieda H., Turner T. J., Awaki H., Koyama K., Mushotzky R., Tsusaka Y., 1990, Nat, 345, 786
Lawrence A., Watson M. G., Pounds K. A., Elvis M., 1987, Nat, 325, 699
Lehto H. J., 1989a, in Hunt J., Battrick B., eds, Two Topics in X-ray Astronomy, ESA SP-296. ESA, Noordwijk, The Netherlands, p. 499
Lehto H., 1989b, PhD thesis, Univ. Virginia
Lehto H., McHardy I. M., Abraham R. G., 1991, in Miller H. M., Wiita P. J., eds, Variability of Active Galactic Nuclei. Cambridge Univ. Press, Cambridge, p. 256
McHardy I. M., 1985, Space Sci. Rev., 40, 559
McHardy I. M., 1988, Mem. Soc. Astron. Ital., 59, 239
McHardy I. M., 1989, in Hunt J., Battrick B., eds, Two Topics in X-ray Astronomy, ESA SP-296. ESA, Noordwijk, The Netherlands, p. 1111
McHardy I. M., Czerny B., 1987, Nat, 325, 696
Madejski G. M., Done D., Turner T. J., Mushotzky R. M., Serlemitsos P., Fiore F., Sikora M., Begelman M. C., 1993, Nat, in press
Papadakis I. E., Lawrence A., 1993, MNRAS, 261, 612
Perley R. A., Schwab F. R., Bridle A. H. (eds), 1985, Synthesis Imaging NRAO. Green Bank, USA, p. 109
Piccinotti G., Mushotzky R. F., Boldt E. A., Holt S. S., Marshall F. E., Serlemitsos P. J., Shafer R. A., 1982, ApJ, 253, 485
Pounds K. A., Turner T. J., 1987, in Treves A., ed., Variability of Galactic and Extragalactic X-ray Sources. Associazione per l'avanzamento dell'astronomia, Bologna, p. 1
Pounds K. A., Stanger V. J., Turner T. J., King A. R., Czerny B., 1987, MNRAS, 224, 443
Pounds K. A., Nandra K., Stewart G. C., George I. M., Fabian A. C., 1990, Nat, 344, 132
Press W. H., 1978, Comments Astrophys., 7, 103
Pudritz R. E., Fahlman G. G., 1982, MNRAS, 198, 689
Rees M. J., 1984, ARA&A, 22, 471
Roberts D. H., Lehar J., Dreher J. W., 1987, AJ, 93, 986
Svensson R., 1987, MNRAS, 227, 403
Tagliaferri G., Stella L., Maraschi L., Treves A., Celotti A., 1991, ApJ, 380, 78
Tennant A. F., Mushotzky R. F., 1983, ApJ, 264, 92
Terlevich R., 1990, in Tenorio-Tagle G., Moles M., Melnick J., eds, Structure and Dynamics of the Interstellar Medium. Springer-Verlag, Berlin, p. 343
Terlevich R., Tenorio-Tagle G., Franco J., Melnick J., 1992, MNRAS, 255, 713
Turner T. J., Pounds K. A., 1989, MNRAS, 240, 833
Unwin S. C., Cohen M. H., Biretta J. A., Pearson T. J., Seielstad G. A., Walker R. C., Simon R. S., Lindfield R. P., 1985, ApJ, 289, 109
Urry C. M., Kruper J. S., Canizares C. R., Rohan M. L., Oberhardt M. R., 1987, in Treves A., ed., Variability of Galactic and Extragalactic X-ray Sources. Associazione per l'avanzamento dell'astronomia, Bologna, p. 15
Vio R., Cristiani S., Lessi O., Provenzale A., 1992, ApJ, 391, 518
Warwick R. S., 1986, in Mason K. O., Watson M. G., White N. E., eds, The Physics of Accretion onto Compact Objects. Springer-Verlag, Berlin, p. 195
Yaqoob T., 1992, MNRAS, 258, 198